
FEW-SHOT CLASS INCREMENTAL LEARNING WITH ATTENTION-AWARE SELF-ADAPTIVE PROMPT

Chenxi Liu, Zhenyi Wang, Tianyi Xiong, Ruibo Chen, Yihan Wu, Junfeng Guo, Heng Huang
University of Maryland, College Park
{cxliu539, zwang169, txiong23, rbchen, ywu42, gjf2023, heng}@umd.edu

ABSTRACT

Few-Shot Class-Incremental Learning (FSCIL) models aim to incrementally learn new classes with scarce samples while preserving knowledge of old ones. Existing FSCIL methods usually fine-tune the entire backbone, leading to overfitting and hindering the potential to learn new classes. On the other hand, recent prompt-based CIL approaches alleviate forgetting by training prompts with sufficient data in each task. In this work, we propose a novel framework named Attention-aware Self-adaptive Prompt (ASP). ASP encourages task-invariant prompts to capture shared knowledge by reducing specific information from the attention aspect. Additionally, self-adaptive task-specific prompts in ASP provide specific information and transfer knowledge from old classes to new classes with an *Information Bottleneck* learning objective. In summary, ASP prevents overfitting on base task and does not require enormous data in few-shot incremental tasks. Extensive experiments on three benchmark datasets validate that ASP consistently outperforms state-of-the-art FSCIL and prompt-based CIL methods in terms of both learning new classes and mitigating forgetting.

Keywords Incremental learning · Few-shot learning · Prompt-based learning

1 Introduction

As the world keeps changing over time, the data in the world also continually changes. Thus, there is a need for machine learning models to follow the data change and continually learn new classes while preserving the knowledge learned from previous data, which is called as Class-Incremental Learning (CIL) [1, 2, 3]. The main challenge of CIL is the catastrophic forgetting problem [4]: a model forgets the previous knowledge after training on new tasks, as the data from old tasks are not fully available due to reasons like limited storage space or privacy issues [5]. While many CIL methods assume a model can continually train on new class data with sufficient samples [6, 7], this assumption does not hold in many real-world applications. For instance, in the scenario of an intelligent medical decision system tracking physiological signals, new patients with limited data must be learned without discarding knowledge from existing patient data [8]. This task of continually learning new classes with limited data is called Few-Shot Class-Incremental Learning (FSCIL) [9, 10]. FSCIL typically involves training a base model using a set of base classes with sufficient data, subsequently utilizing the knowledge learned from base classes to facilitate the incremental learning of new classes with limited data. Beyond the challenge of catastrophic forgetting, FSCIL also triggers overfitting on limited training samples, making it harder for a machine model to learn new classes.

Various works [9] have been proposed to address the FSCIL scenario. Some of them focus on enhancing base models' ability to generalize across newly encountered few-shot classes [11, 12, 13], while others aim to find a better strategy to incrementally train on new tasks with limited data [14, 15, 16, 17]. However, most existing works fine-tune all the parameters in the base model, which leads to overfitting on base classes and hinders the transferability to new classes. On the other hand, recent prompt-based CIL methods [18, 19, 20] leverage the inherent generalization ability of large pre-trained Vision Transformer (ViT) [21] by fixing the backbone parameters and only training a few new parameters called prompts [22, 23]. They usually learn task-specific prompts via a key-query mechanism and store the knowledge of seen tasks in a specialized prompt pool. In this way, they preserve the knowledge of old tasks without necessitating a rehearsal buffer to store old data samples. Nonetheless, to train the task-specific prompts, prompt-based approaches require the model to be trained on sufficient data samples, which are not available in few-shot incremental tasks.

In this paper, we propose a novel Attention-Aware Self-Adaptive Prompt (ASP) framework to overcome the shortcomings of existing FSCIL and prompt-based CIL methods under the FSCIL setting. Aiming to facilitate the continual learning of new classes with limited data, ASP leverages the inherent generalization capability of the pre-trained ViT and utilizes the knowledge learned from sufficient base classes. Specifically, ASP fixes the ViT backbone and introduces prompts between attention blocks for adapting to FSCIL tasks, where prompts are decomposed into attention-aware task-invariant prompts (TIP) and self-adaptive task-specific prompts (TSP). The attention blocks pay the same attention to each TIP regardless of the task, encouraging TIP to only contain task-invariant information that can be universally used for both base classes and new classes. Unlike the previous key-query mechanics, ASP uses a prompt encoder to convert input images to prompt features. Inspired by the *Information Bottleneck* (IB) theory [24], ASP guides the prompt encoder to generate prompt features that have a strong correlation with semantic information and a weak correlation with extraneous information contained in images. To further improve the generalization ability, ASP aggregates prompt features over the training set to prevent overfitting on a single input image. For a specific input image, the corresponding TSP is composed of the average prompt features and its own prompt features. Consequently, ASP avoids fine-tuning the entire backbone to alleviate overfitting and circumvents the need of sufficient data to train new TSP for new classes. Lastly, to further enhance model discrimination, a similarity-based loss is used to cluster feature vectors to their class centers, where class centers are estimated by the anchor samples during training.

Overall, our contributions can be summarized as below:

- We propose ASP, an innovative prompt-based methodology to address both the overfitting challenge in existing FSCIL methods and the data-hungry drawback in existing prompt-based methods under the FSCIL scenario.
- We design attention-aware TIP and self-adaptive TSP to transfer knowledge from base classes to new classes and alleviate forgetting on previously learned classes.
- We conduct extensive experiments on three benchmark datasets to demonstrate that ASP substantially outperforms SOTA FSCIL and prompt-based CIL methods in both learning new classes and preserving performance on old classes.

2 Related Work

2.1 Class-Incremental Learning

Non-prompt-based approaches: In general, there are three different settings of incremental learning: task-, domain, and class-incremental learning (TIL, DIL, and CIL) [1]. Among all, CIL is considered to be the most challenging scenario [9], which is required to learn new classes without forgetting old ones. In current CIL works, there are three main directions. The most effective one is rehearsal methods [25, 26, 27, 28, 29], which build a rehearsal buffer to store samples from previous tasks. The second direction is to find out important parameters for the current task and prevent them from changing over incremental tasks [30, 31, 32]. In addition, a lot of works utilize knowledge distillation to preserve the knowledge of previous tasks to overcome forgetting [33, 6, 25]. Recently, some rehearsal-free methods [34, 19] have caught people’s attention, as rehearsal samples are not always allowed to be stored in real-world scenarios [18]. Notably, ASP also doesn’t need a rehearsal buffer to store any data samples. Typically, CIL methods require enough training data in each incremental task to learn new classes, which is not available under the FSCIL scenario.

Prompt-based approaches: Prompt-based methods [22, 23] are first proposed for Natural Language Processing tasks, which can better utilize the pre-trained knowledge for downstream tasks. The basic idea is fixing the backbone parameters and only fine-tuning a few new parameters (prompts) prepend to input text or images [35]. Recently, prompt-based CIL approaches using ViT backbones achieve significant performance in both learning new classes and preventing catastrophic forgetting. L2P [18] first proposes to use a key-query mechanism to select task-specific prompts from a prompt pool. DualP [19] adds task-invariant prompts to capture the shared information among tasks. But their task-invariant prompts still provide much task-specific information and their task-specific prompts require sufficient training data in incremental tasks. This would result in significant overfitting to new few-shot incremental tasks because of the limited availability of new task data, ultimately causing a decline in performance for FSCIL. Subsequently, CodaP [20] proposes to train the prompt pool and selection mechanism in an end-to-end manner. The most recent HideP [36] decomposes CIL into hierarchical components and optimizes them respectively. However, all existing prompt-based CIL methods are not suitable under the FSCIL scenario, as they all need sufficient data samples in incremental tasks to capture task-specific knowledge and store them in prompts. Reversely, ASP does not need to train new task-specific prompts for new tasks and thus works well in few-shot incremental tasks.

2.2 Few-Shot Class-Incremental Learning

Few-Shot Class-Incremental Learning (FSCIL) is even more challenging than normal CIL, as it needs to incrementally learn new classes with limited labeled data [9]. TOPIC [37] first proposed the FSCIL task, which is required to first obtain a base model trained on sufficient base classes, then incrementally learn some new tasks with limited new class data. Current FSCIL methods can be roughly divided into two groups. The first group aims to utilize base classes to train a generalized backbone that can be transferred to few-shot incremental tasks [11, 12, 13]. The trained backbone is usually kept frozen during the following few-shot incremental tasks [38, 39, 40]. The second group focuses on the strategy of incrementally learning few-shot new classes without overfitting [14, 15, 16]. These FSCIL methods usually fine-tune all parameters in the backbone when training on base classes, which leads to overfitting on base classes and hinders the transferability to new classes. In contrast, ASP fixes the pre-trained backbone and stores task-invariant knowledge in prompts to overcome this issue.

3 Preliminaries

Few-shot Class-incremental Learning aims to learn a sequence of tasks t using their respective data $\mathcal{D}_0, \dots, \mathcal{D}_T$. When learning on task t , data from previous tasks $0, \dots, t-1$ are totally unavailable or only partially available, and the model is required to perform well on all seen tasks $0, \dots, t$. The training data in task t is represented as $\mathcal{D}_t = \{(\mathbf{x}_{t,i}, y_{t,i})\}_{i=1}^{N_t}$, where $N_t = |\mathcal{D}_t|$ denotes the size of \mathcal{D}_t , $\mathbf{x}_{t,i} \in \mathcal{X}_t$ and $y_{t,i} \in \mathcal{Y}_t$ represent the sample and label, respectively. The training label spaces between different tasks are disjoint, i.e., for any task $t, t' \in [0, T]$ and $t \neq t'$, $\mathcal{Y}_t \cap \mathcal{Y}_{t'} = \emptyset$. The first task has sufficient training data \mathcal{D}_0 and is called the base task, while the following incremental tasks can be denoted as N -way K -shot classification tasks, i.e., N classes for each task and K samples for each class. A FSCIL model can be decoupled into a backbone f_θ parameterized by θ , and a linear classifier h_ψ parameterized by ψ . For an input test data \mathbf{x} drawn from all seen tasks, the model tries to predict $y = h_\psi(f_\theta(\mathbf{x}))$ which matches the class label.

Prompt-based Approaches for vision tasks typically use a pre-trained vision transformer (ViT) [21] as the backbone f_θ , and the parameter θ are typically frozen during training to maintain the generalization ability obtained from the pre-training. A ViT model contains multiple multi-head self-attention (MSA) layers, and we denote the input of the l^{th} MSA layer as $\mathbf{h}^l \in \mathbb{R}^{L_h \times D}$, then the output of this layer is given as:

$$\text{MSA}(\mathbf{h}^l) = \text{Concat}(h_1^l, \dots, h_m^l)W^O \quad (1)$$

$$h_i^l = \text{Attention}(\mathbf{h}^l W_i^Q, \mathbf{h}^l W_i^K, \mathbf{h}^l W_i^V), i = 1, \dots, m \quad (2)$$

$$\text{Attention}(Q, K, V) = \text{softmax}\left(\frac{QK^T}{\sqrt{d_k}}\right)V \quad (3)$$

where W^O, W_i^Q, W_i^K, W_i^V are projection matrices, m is the number of attention heads and d_k is a scaling factor. Among prompt-based approaches, Prompt Tuning (ProT) [22, 35] is one of the most commonly used techniques which introduce a few trainable parameters $\mathbf{p}^l \in \mathbb{R}^{L_p \times D}$ as prompts for the l^{th} layer, and these prompts are prepend to \mathbf{h}^l :

$$f_{\text{ProT}}(\mathbf{p}^l, \mathbf{h}^l) = \text{MSA}([\mathbf{p}^l; \mathbf{h}^l]) \quad (4)$$

where $[\cdot; \cdot]$ denotes the concatenation operation along the dimension of sequence length. Before the first layer of ViT, an input image is first split as a few patches and transformed into a sequence-like representation $\mathbf{x}^e \in \mathbb{R}^{L_x \times D}$. For image classification tasks [35], a class token $\mathbf{cls} \in \mathbb{R}^{1 \times D}$ is prepend and the visual prompts are prepend to form the input of ViT blocks:

$$\mathbf{x}^p = [\mathbf{cls}; \mathbf{p}^0; \mathbf{x}^e] \quad (5)$$

Prototypical Network [41] is a widely used approach for few-shot learning problems. It calculates the mean features \mathbf{c}_k of a class k and uses it as the class prototype:

$$\mathbf{c}_k = \frac{1}{N_k} \sum_{y_i=k} f(\mathbf{x}_i) \quad (6)$$

where N_k is the number of samples in class k , and the output feature of the \mathbf{cls} token is used as the image embedding. For a classification task with K classes, $W = [\mathbf{c}_0, \mathbf{c}_1, \dots, \mathbf{c}_K]$ is used as the linear classifier, and an input sample is classified via the softmax probability with class prototypes: $P(y = k|\mathbf{x}) \propto \mathbf{c}_k^T f_{\theta, \mathbf{p}}(\mathbf{x})$. Following works [42, 43], new class prototypes are append to W to perform classification over all seen classes.

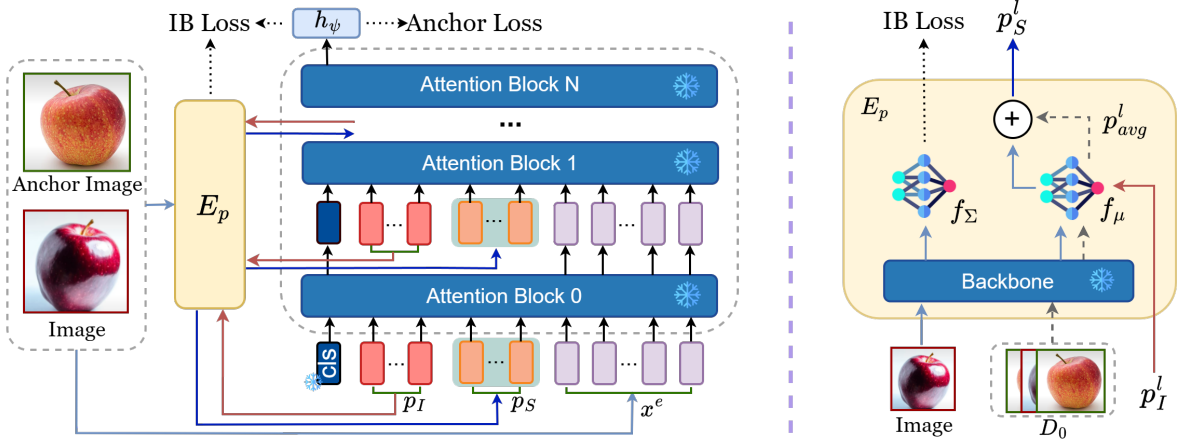


Figure 1: Overall training scheme of ASP for the base task. For incremental tasks where $t > 0$, ASP updates only p_{avg} using Equation 13. **Left:** The pre-trained backbone remains frozen during training and the prompts are inserted into layers between attention blocks. The TIP p_I are initialized from an attention-aware aspect, while the TSP p_S are derived from the prompt encoder E_p . At the beginning of each training epoch, anchor images are selected using Equation 18. Throughout the training, the prompts and E_p are optimized using IB loss and Anchor loss as specified in Equation 19. **Right:** Details of the prompt encoder E_p . Image features extracted by the frozen pre-trained backbone are fed to two tiny networks f_μ and f_Σ . At the start of each training epoch, p_{avg} is calculated via Equation 12 using p_I and all data in the base task. Within a training epoch, the output of f_Σ contributes to IB loss, while p_S results from blending p_{avg} and the output of f_μ , as outlined in Equation 11.

4 Methodology

A base model with good generalization ability is beneficial for adapting to few-shot new classes [43, 38]. To prevent overfitting on base classes after sufficient training, and to leverage the generalization ability of pre-trained ViT for learning new classes with limited data, ASP fixes the pre-trained backbone and learns prompts that can transfer the knowledge learned from base classes to new classes. Inspired by DualP [19], we decompose the prompts into attention-aware task-invariant prompts and self-adaptive task-specific prompts. In Section 4.1, ASP maintains consistent attention across all task-invariant prompts for any given task, thereby containing minimal task-specific information. In Section 4.2, ASP employs a prompt encoder to map an input image to TSP leveraging the *Information Bottleneck* theory, which has been proven to enhance generalization ability [44]. Thus, the prompt encoder can also be used for new class data without further training. Finally, Section 4.3 introduces an Anchor Loss, which enlarges class margins by pulling class features toward their class centers, thereby further improving model discrimination ability. ASP only trains the model on the base task using sufficient data from base classes. Subsequently, the prompts are updated using Equation 13 for few-shot incremental tasks. Overall, our training scheme is shown in Figure 1.

4.1 Attention-Aware Task-Invariant Prompts

Similar to DualP [19], task-invariant prompts are fixed after training on base classes and used for subsequent few-shot incremental tasks. Despite DualP employing the same task-invariant prompts for all tasks, it is not true that they convey identical information across different tasks due to the difference of attention on each prompt token. Consequently, these task-invariant prompts continue to offer task-specific information. To diminish the task-specific information stored in prompts, ASP promotes consistent attention weight on each prompt token. The attention on different tokens can be measured by the attention matrix $A = \text{softmax}(\frac{QK^T}{\sqrt{d_k}})$. Denote the i^{th} token in layer h^l as $\mathbf{t}_i \in \mathbb{R}^{1 \times D}$, the attention from the i^{th} token to j^{th} token is:

$$A_{ij} = \frac{\exp(\mathbf{t}_i W^Q \cdot \mathbf{t}_j W^K)}{\sum_{m=1}^{1+L_p+L_x} \exp(\mathbf{t}_i W^Q \cdot \mathbf{t}_m W^K)} \quad (7)$$

The attention is conditioned on the value of the prompt token, and the same attention can be guaranteed if two prompt tokens have the same values. The simplest way is initializing each prompt token with the same value before training, and the values will keep the sample during the model update using gradient decent algorithms [45]. In the base class training task, we use prompts $p_I^l \in \mathbb{R}^{L_{p_I} \times D}$ where each token is initialized using the same values as the task-invariant prompt. The comparison between our attention-aware TIP and widely used randomly initialized prompt is shown in

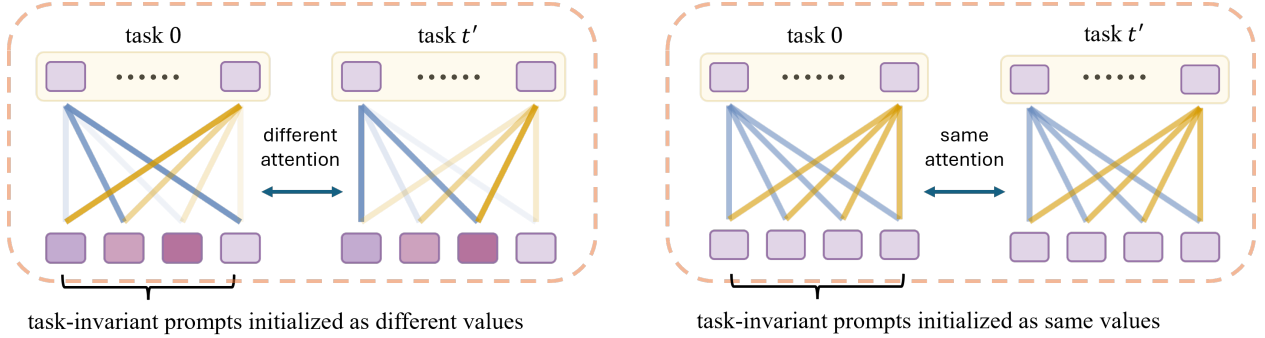


Figure 2: Attention on task-invariant prompts between different tasks. A deeper line color indicates greater attention. **Left:** When initialized with different values, attention on each prompt differs across tasks, thereby providing inconsistent information. **Right:** ASP initializes TIP with the same values, ensuring consistent attention across tasks and providing uniform information.

Figure 2. As p_i^l always contribute the same to the model output regardless of task and image class, it is encouraged to contain knowledge shared among all base classes. This class-invariant knowledge can also be used for new classes in incremental tasks, thus it is also task-invariant knowledge. After training on base classes, the TIP are fixed during few-shot incremental tasks.

4.2 Self-Adaptive Task-Specific Prompts

However, relying solely on TIP may lead to underfitting, as it only considers the shared attributes across different tasks and ignores the unique attributes. To incorporate task-specific information into prompts, prior studies [18, 19] introduce a key-query mechanism to generate task-specific prompts based on input images. However, these methods require a large amount of training data to capture the task-specific information and store it in prompts. In contrast, ASP utilizes a compact neural network as a prompt encoder E_p to convert input images to task-specific prompts. This prompt encoder is initially trained with sufficient base class data to acquire encoding capabilities. To ensure these capabilities are extendable to new classes, ASP enhances the generalization ability of the prompt encoder by adopting principles from the *Information Bottleneck* theory [24].

Prompt Learning Objective Inspired by IB theory [24], we propose the following learning objective for prompt learning:

$$\mathcal{L}_{IB} = I(\mathcal{P}; \mathcal{X}) - \gamma I(\mathcal{P}; \mathcal{Y}) \quad (8)$$

We utilize the random variable \mathcal{P} to represent the latent prompt associated with input \mathcal{X} . The mutual information between the latent prompt \mathcal{P} and data labels \mathcal{Y} is denoted as $I(\mathcal{P}; \mathcal{Y})$, while $I(\mathcal{P}; \mathcal{X})$ denotes the mutual information between latent prompt \mathcal{P} and input data \mathcal{X} . Here, γ is a constant. In Equation 8, the term $I(\mathcal{P}; \mathcal{X}) - \gamma I(\mathcal{P}; \mathcal{Y})$ constitutes the *Information Bottleneck* (IB) loss. Maximizing the mutual information between \mathcal{P} and \mathcal{Y} aims to strengthen the correlation between them, thereby capturing semantic knowledge. Conversely, minimizing the mutual information between \mathcal{X} and \mathcal{P} aims to mitigate the influence of extraneous information from input \mathcal{X} on the prompt \mathcal{P} , thereby enhancing generalization. However, computing the mutual information is generally intractable since it often necessitates integration over the joint distribution of the involved variables. This integration poses computational or analytical challenges. Variational inference offers a framework for approximating these intractable integrals. We formulate the variational lower bound as follows:

$$\begin{aligned} I(\mathcal{P}; \mathcal{Y}) - \gamma I(\mathcal{P}; \mathcal{X}) &\geq \int P(\mathbf{x})P(\mathbf{y}|\mathbf{x})P(\mathbf{p}|\mathbf{x}) \log P(\mathbf{y}|\mathbf{p})d\mathbf{x}d\mathbf{y}d\mathbf{p} \\ &- \gamma \int P(\mathbf{x})P(\mathbf{p}|\mathbf{x}) \log \frac{P(\mathbf{p}|\mathbf{x})}{r(\mathbf{p})}d\mathbf{x}d\mathbf{p} \end{aligned} \quad (9)$$

Here, $r(\mathbf{p})$ serves as a variational marginal approximation of the intractable marginal $P(\mathbf{p})$, and it is chosen as $r(\mathbf{p}) = \mathcal{N}(0, I)$. The detailed derivation steps are provided in the Appendix.

We now delve into the calculation of Equation 9. The term $P(\mathbf{y}, \mathbf{x}) = P(\mathbf{x})P(\mathbf{y}|\mathbf{x})$ is approximated by the empirical data distribution $P(\mathbf{x}|\mathbf{y}) = \frac{1}{N} \sum_{n=1}^N \delta_{\mathbf{x}_n}(\mathbf{x})\delta_{\mathbf{y}_n}(\mathbf{y})$, where $\delta_{\mathbf{x}_n}$ and $\delta_{\mathbf{y}_n}$ represent the Dirac delta function. Assuming the prompt encoder E_p follows the form: $P(\mathbf{p}|\mathbf{x}) = \mathcal{N}(\mathbf{p}|f_\mu(\mathbf{x}), f_\Sigma(\mathbf{x}))$ where two fully connected networks f_μ and f_Σ outputs the K -dimensional mean μ of \mathbf{p} and the $K \times K$ covariance matrix Σ . Then, employing the reparameterization trick [46, 47], we rewrite $P(\mathbf{y}|\mathbf{x})d\mathbf{p}$ as $P(\epsilon)d\epsilon$. By calculating the Kullback-Leibler (KL) divergence between $P(\mathbf{p}|\mathbf{x})$

and $r(\mathbf{p})$, and combining all components, we obtain the empirical *Information Bottleneck* loss function as described in Equation 10, which we aim to minimize.

$$\mathcal{L}_{IB} = \mathbb{E}_{\epsilon \sim \mathcal{N}(0, I)}[-\log P(y|\mathbf{x}, \epsilon)] + \mathbb{KL}(P(\mathbf{p}|\mathbf{x})|r(\mathbf{p})) \quad (10)$$

We use the prompt encoder E_p to convert an image to the corresponding TSP. Inspired by previous works [18, 19], E_p first uses the pre-trained backbone f_θ to extract the embedding features of input images and then fed to f_μ to obtain prompt features. Aiming to transfer the knowledge learned from base classes to new classes, the prompt encoder also takes TIP as input to generate TSP. To further improve the generalization ability of our TSP for new classes, we consider all prompt features obtained from \mathcal{X}_0 to provide general information together with the prompt features of an input image to construct the corresponding task-specific prompts \mathbf{p}_S . In this way, \mathbf{p}_S can avoid overfitting to a single input image and become easier to generalize to unseen classes. During the base class training stage, the task-specific prompts for layer l are given as:

$$\mathbf{p}_S^l = \alpha \mathbf{p}_{avg}^l + (1 - \alpha) f_\mu([\mathbf{p}_I^l; f_\theta(\mathbf{x} + \epsilon)]) \quad (11)$$

$$\mathbf{p}_{avg}^l = \frac{1}{N_0} \sum_{N_0} f_\mu([\mathbf{p}_I^l; f_\theta(\mathbf{x}_0)]) \quad (12)$$

where α is a hyperparameter. \mathbf{p}_{avg}^l is the average prompt features of data in the base task, which is recalculated at the beginning of each training epoch. For incremental task t , information of new classes is incorporated into \mathbf{p}_{avg}^l using Exponential Moving Average (EMA) [48]:

$$\mathbf{p}_{avg}^l = \beta \mathbf{p}_{avg}^l + (1 - \beta) \frac{1}{N_t} \sum_{N_t} f_\mu([\mathbf{p}_I^l; f_\theta(\mathbf{x}_t)]) \quad (13)$$

where β is a hyperparameter to control the adapting speed. During the testing phase, noise ϵ is removed from the Equation 11 to generate TSP. To balance the influence of task-invariant and task-specific prompts, their prompt length is set as the same, i.e. $L_{\mathbf{p}_S} = L_{\mathbf{p}_I}$. Finally, the prompts inserted into layer l is:

$$\mathbf{p}^l = [\mathbf{p}_I^l; \mathbf{p}_S^l] \quad (14)$$

4.3 Anchor Loss

In the base classes training stage, we aim to obtain a feature extractor that can (1) maximize the distance between inter-class feature embeddings, and (2) minimize the distance between intra-class feature embeddings. Furthermore, we also want to obtain a classifier head h_ψ that can accurately classify these features into class predictions. Following previous works [40, 42], we use a fully connected layer without bias term as the classifier head h_ψ , and the prediction is obtained by measuring the cosine similarity between feature embeddings and weights W in the classifier head:

$$y_k = \frac{W_k^T f_{\theta, \mathbf{p}}(\mathbf{x} + \epsilon)}{\|W_k\| \cdot \|f_{\theta, \mathbf{p}}(\mathbf{x} + \epsilon)\|} \quad (15)$$

where $\|\cdot\|$ is l_2 normalization. The noise term ϵ is removed in the testing phase and the weight W_k can be seen as the prototype of class k [40, 49]. To separate class features and prototypes, the Cross-Entropy loss is used as the first term in Equation 10:

$$\mathcal{L}_{IB} = -\frac{1}{N} \sum_N \log \frac{\exp(y_k)}{\sum_{k' \in K} \exp(y_{k'})} + \mathbb{KL}(P(\mathbf{p}|\mathbf{x})|r(\mathbf{p})) \quad (16)$$

The Cross-Entropy loss simultaneously pulls class features $f_{\theta, \mathbf{p}}(\mathbf{x}_k)$ to its class prototype W_k , and pushes far away from other class prototypes $W_{i \neq k}$. However, only the pull action is accurate while the push action may lead the class prototype to diverge from the class mean and cause misclassification. Similar to previous works [42, 50], we replace W with class mean \mathbf{c} after training on base classes. Therefore, it is necessary to align class features with their class mean, which can also reserve places for new classes to improve new class accuracy [43, 38]. For any input sample, we maximize the cosine similarity between its features and the corresponding class mean:

$$\mathcal{L}_c = 1 - \frac{\mathbf{c}_k^T f_{\theta, \mathbf{p}}(\mathbf{x}_k)}{\|\mathbf{c}_k\| \cdot \|f_{\theta, \mathbf{p}}(\mathbf{x}_k)\|} \quad (17)$$

As the class mean keeps changing during the training process, it is resource-consuming to compute the accurate class mean after each mini-batch. Thus, we propose to use an anchor sample to estimate the class mean. At the beginning of

each training epoch, the accurate class mean is computed, and the sample that has the largest similarity with the class mean is selected as the anchor sample for that class:

$$\hat{\mathbf{x}}_k = \arg \max_{\mathbf{x} \in \mathcal{X}_k} \frac{\mathbf{c}_k^T f_{\theta, \mathcal{P}}(\mathbf{x})}{\|\mathbf{c}_k\| \cdot \|f_{\theta, \mathcal{P}}(\mathbf{x})\|} \quad (18)$$

Then the estimated class mean for L_c is $\hat{\mathbf{c}}_k = f_{\theta, \mathcal{P}}(\hat{\mathbf{x}}_k)$. Overall, the final training loss is:

$$\mathcal{L} = \mathcal{L}_{IB} + \lambda \mathcal{L}_c \quad (19)$$

where λ is a hyperparameter.

5 Experiments

In this section, we first introduce the experiment details of FSCIL, including datasets, evaluation protocol, training details, and baseline methods. Subsequently, we compare ASP with baselines on three benchmark datasets, which show the effectiveness of ASP. In addition, the ablation study verifies the effectiveness of different components in ASP. Lastly, we provide more experimental results for further analysis. We will release our code after the paper decision.

5.1 Implementation Details

Datasets: Following the previous FSCIL works [43, 42] and prompt-based CIL works [19, 36], we evaluate the performance on CIFAR100 [51], CUB200-2011 [52], and ImageNet-R [53] dataset. Similar to prior studies [43, 42], the datasets are split to form the FSCIL tasks. In detail, CIFAR100 is divided into 60 base classes and 40 new classes. The new classes are further divided into eight 5-way 5-shot incremental tasks. CUB200 and ImageNet-R are divided into 100 classes for the base task, and the left 100 classes are divided into ten 10-way 5-shot incremental tasks.

Evaluation protocol: Following previous works [10, 43, 13], we denote the Top-1 accuracy on all seen tasks $0, \dots, t$ after the t -th task as A_t . The average accuracy $A_{avg} = \frac{\sum_{t=0}^T A_t}{T+1}$ measures the overall performance during all incremental tasks. And the forgetting phenomenon is measured by the performance dropping rate (PD), i.e., $PD = A_0 - A_T$, where 0 stands for the base task and T stands for the last task. Furthermore, Harmonic Accuracy (HAcc) [40] is used to reflect the balanced performance across both base and new classes after task T : $A_h = \frac{2 \times A_o \times A_n}{A_o + A_n}$, where A_o is the accuracy of base class in task 0 and A_n is the average accuracy of all classes in tasks $t > 0$.

Training details: All experiments are conducted with PyTorch [54] on NVIDIA RTX A6000. We follow works [20, 50] to choose ViT-B/16-1K [21], which pre-trained on ImageNet1K as the backbone f_θ . For all datasets, the input images are resized to 224×224 and trained 20 epochs using SGD optimizer. The learning rate is set as 0.01 for CIFAR100 and CUB200 while 0.03 is used for ImageNet-R. We use batch size of 48 for CIFAR100 and batch size of 24 for both CUB200 and ImageNet-R. The prompt token length $L_{p_g} = L_{p_d}$ of 10 is used for ImageNet-R, and 3 for CIFAR100 and CUB200. All experiments are run using three random seeds and the average results are reported.

Baselines: We first compare two widely used CIL methods iCaRL [25] and Foster [55]. Besides, we also compare the SOTA FSCIL algorithms: CEC [39], FACT [43] and TEEN [42]. Lastly, we compare the recent SOTA prompt-based CIL approaches: L2P [18], DualP [19], and CodaP [20].

5.2 Benchmark Comparisons

In this section, we report the performance of baselines and ASP under FSCIL setting. For CIFAR100 and ImageNet-R, the detailed accuracy in each task and the three evaluation metrics are shown in Table 1 and Table 2. The detailed performance of CUB200 can be found in the appendix. Furthermore, the performance curves of the Top-1 accuracy A_t in each incremental task under all three datasets are shown in Figure 3.

Based on the experimental results on CIFAR100, CUB200 and ImageNet-R, ASP achieves the best Top-1 accuracy A_T of 86.7%, 83.5% and 69.7%, surpassing the second best by 2.7%, 2.9% and 7.2% respectively. Furthermore, ASP usually performs the best on A_t before the last task, except the first task. In the first task, classical CIL and FSCIL methods fine-tune all the parameters using sufficient data, thus it is reasonable that they perform better than the prompt-based CIL approaches. Besides, ASP performs the best on the average accuracy A_{avg} , which achieves 89.0%, 83.8% and 75.3% and surpasses the second best by 1.7%, 0.7% and 9.2% on three benchmark datasets respectively. In addition, ASP achieves the lowest PD on CIFAR100 and CUB200 while achieving the second lowest on ImageNet-R. For the HAcc metric, ASP also achieves the best of 85.3%, 83.4% and 67.0% on three benchmark datasets, which can

Table 1: Detailed Top-1 accuracy A_t in each incremental task, average accuracy A_{avg} , performance dropping rate (PD) and Harmonic Accuracy (HAcc) on CIFAR100 dataset. \uparrow means higher is better, and \downarrow means lower is better.

Method	Accuracy A_t in each task (%) \uparrow										A_{avg} \uparrow	PD \downarrow	HAcc \uparrow
	0	1	2	3	4	5	6	7	8				
iCaRL	94.2	88.9	84.7	80.0	74.9	75.6	71.8	68.2	67.1	78.4	27.2	57.5	
Foster	94.2	88.3	81.6	77.0	72.8	67.9	64.4	60.9	58.3	73.9	35.9	11.0	
CEC	91.6	88.1	85.3	81.7	80.2	78.0	76.5	74.8	72.6	81.0	19.0	64.1	
FACT	91.0	87.2	83.5	79.7	77.2	74.8	73.1	71.6	69.4	78.6	21.7	55.5	
TEEN	92.9	90.2	88.4	86.8	86.4	86.0	85.8	85.1	84.0	87.3	8.8	81.2	
L2P	92.2	85.2	79.2	73.8	69.2	65.1	61.4	58.1	55.2	71.1	37.0	0.0	
DualP	91.8	84.7	78.6	73.3	68.7	64.6	61.1	57.8	54.9	70.6	36.9	0.1	
CodaP	93.4	86.2	80.1	74.7	70.1	66.0	62.3	59.0	56.0	72.0	37.4	0.0	
L2P+	84.7	82.3	80.1	77.5	77.0	76.0	75.6	74.1	72.3	77.7	12.4	68.0	
DualP+	86.0	83.6	82.9	80.2	80.6	80.2	80.5	79.0	77.4	81.1	8.5	75.3	
CodaP+	86.0	83.6	81.6	79.2	79.1	78.5	78.3	77.0	75.4	79.9	10.6	72.2	
Ours	92.2	90.7	90.0	88.7	88.7	88.2	88.2	87.8	86.7	89.0	5.5	85.3	

Table 2: Detailed Top-1 accuracy A_t in each incremental task, average accuracy A_{avg} , performance dropping rate (PD) and Harmonic Accuracy (HAcc) on ImageNet-R dataset. \uparrow means higher is better, and \downarrow means lower is better.

Method	Accuracy A_t in each task (%) \uparrow											A_{avg} \uparrow	PD \downarrow	HAcc \uparrow
	0	1	2	3	4	5	6	7	8	9	10			
iCaRL	80.6	69.2	59.0	52.8	49.4	45.5	42.8	42.3	40.5	40.1	39.4	51.0	41.2	36.1
Foster	85.8	78.8	71.8	67.4	63.1	58.5	55.9	53.8	51.5	49.3	47.0	62.1	38.7	36.8
CEC	79.4	71.9	69.0	64.1	60.4	58.6	56.4	53.2	52.0	50.0	48.3	60.3	31.1	32.6
FACT	79.4	72.5	69.0	63.8	60.1	57.6	54.7	52.2	50.2	48.1	46.0	59.4	33.4	22.3
TEEN	84.6	76.7	68.8	67.6	64.3	60.6	58.3	56.1	56.1	54.7	54.9	63.9	29.7	45.4
L2P	80.4	73.0	67.8	62.3	58.0	55.1	52.0	48.3	45.8	42.9	40.6	56.9	39.8	1.0
DualP	75.6	68.5	63.8	58.7	54.7	52.2	49.4	46.0	43.8	41.1	39.0	53.9	36.7	2.7
CodaP	82.1	74.4	69.4	64.1	59.8	57.1	53.9	50.5	48.2	45.3	43.2	58.9	38.9	6.5
L2P+	73.9	70.9	69.3	65.9	64.0	62.6	60.1	59.5	59.0	58.2	56.8	63.7	17.2	52.0
DualP+	71.5	69.0	69.0	67.4	66.6	65.9	64.1	64.0	64.0	63.4	62.5	66.1	9.0	61.6
CodaP+	74.4	69.3	67.7	63.7	62.0	61.3	58.5	58.2	57.5	54.7	55.3	62.0	19.1	54.5
Ours	83.3	80.4	79.6	77.0	75.6	74.7	73.0	72.1	71.9	70.9	69.7	75.3	13.5	67.0

demonstrate the superiority of ASP in incrementally learning new classes while preserving performance on base classes at the same time.

Interestingly, we find that prompt-based CIL approaches learn nearly nothing about the new classes based on the HAcc metric. We think the main reason may be the severe overfitting of few-shot data in the classifier head, which is a fully connected layer. Thus, we replace the original classifier head with the class mean to form a prototypical network, which is denoted as L2P+, DualP+, and CodaP+. The HAcc results in Table 1 and Table 2 show that this modification largely improves their ability to learn new tasks under the FSCIL setting.

5.3 Ablation Study

We conduct ablation study on three benchmark datasets, and the implementation details are the same as the setting in Section 5.1. To verify the effectiveness of each component in ASP, we alternatively remove each component from the framework and measure the average accuracy A_{avg} . The results are shown in Table 3, where *ours w/o TIP* refers to removing the attention-aware task-invariant prompt p_I from our framework, *ours w/o TSP* refers to removing the self-adaptive task-specific prompt p_S from our framework, *ours w/o \mathcal{L}_c* refers to removing the anchor loss \mathcal{L}_c from our framework. Finally, *ours w/ Diff TIP* means we use a Gaussian distribution to initialize different values for each task-invariant prompt. The results show that removing any component leads to a performance drop in the average accuracy A_{avg} , which demonstrates the effectiveness of our design.

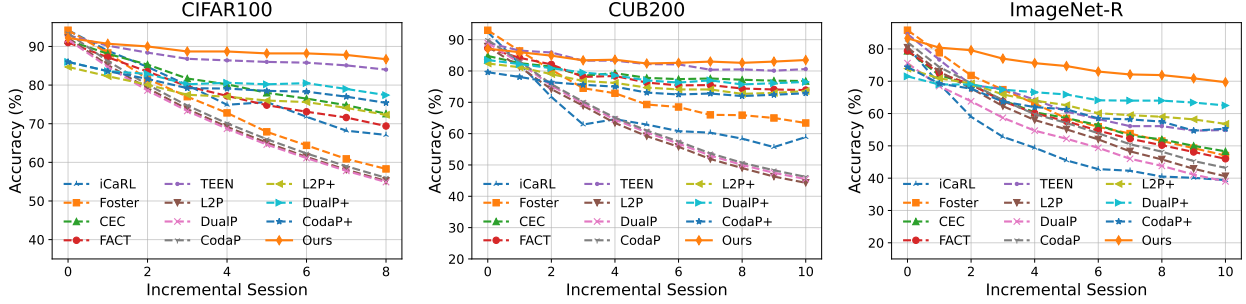


Figure 3: Detailed Top-1 accuracy A_t in each incremental task on three benchmark datasets. ASP outperforms baselines in most tasks.

Table 3: Ablation study of removing each component from ASP respectively. The average accuracy A_{avg} is reported on three benchmark datasets.

Methods	A_{avg}		
	CIFAR100	CUB200	ImageNet-R
Ours w/o TIP	88.5	83.4	72.2
Ours w/o TSP	88.1	83.0	73.9
Ours w/o \mathcal{L}_c	88.6	83.2	74.5
Ours w/ Diff TIP	87.6	82.6	73.3
Ours	89.0	83.8	75.3

Table 4: Influence of the Incremental Shot on average accuracy A_{avg} on three benchmark datasets.

Methods	A_{avg}		
	CIFAR100	CUB200	ImageNet-R
1-shot	82.9	78.6	69.3
5-shot	89.0	83.8	75.3
10-shot	90.0	85.3	76.6
20-shot	90.3	85.8	77.4

5.4 Further Analysis

Hyper-Parameter: We conduct sensitive analysis of α , β , λ and prompt length $L_g = L_d$. The same experimental setting of 10-way 5-shot is used on the ImageNet-R dataset and the results are shown in Figure 4. To achieve the highest A_{avg} , we choose $\alpha = 0.8$, $\beta = 0.99$ and $\lambda = 0.1$ for all benchmark datasets. The prompt length is set as 3 for CIFAR100 and CUB200 while is set as 10 for ImageNet-R.

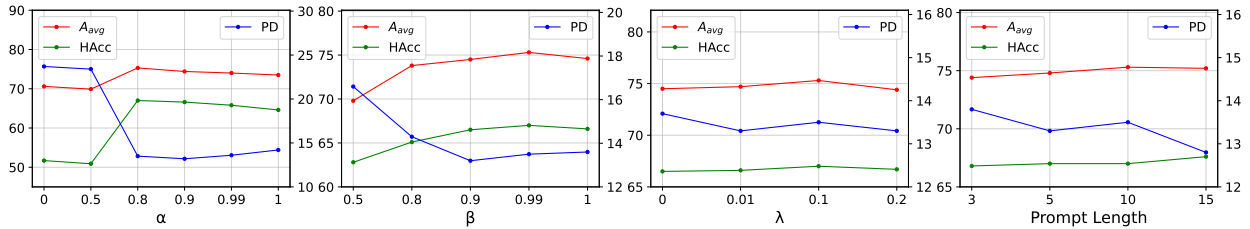


Figure 4: Sensitive analysis of α , β , λ and prompt length $L_g = L_d$. The average accuracy A_{avg} is reported on ImageNet-R datasets.

Incremental Shot: ASP learns new classes using K -shot data, and we change the shot to find out the data influence on the average accuracy A_{avg} . The experimental setting is the same with Section 5.2 and 1, 10, 20-shot of new classes are provided in incremental tasks on three datasets. The results in Table 4 show that more available samples per class in incremental tasks can help improve the model performance. However, we also find that the performance improvement becomes smaller as we increase shot K .

Task-Specific Prompts: The effectiveness of the self-adaptive task-specific prompts module is validated in Section 5.3, and we provide further analysis to evaluate the importance of the average prompt features p_{avg} in Equation 12 and the EMA in Equation 13. We remove p_{avg} by setting $\alpha = 0$ and don't update p_{avg} for new tasks by setting the EMA parameter β as 1. Based on the results in Figure 4, both cases lead to performance drop on A_{avg} , PD and HACC, which validates the effectiveness of p_{avg} and EMA.

Base&New Class Accuracy: Except HAcc metrics, we provide the detailed accuracy of the base classes from task 0 and the new classes from task $t > 0$ after the last task T . The results of baselines and ASP are shown in Figure 5. ASP outperforms all baselines in terms of learning new classes using few-shot data while achieving competitive performance in maintaining performance on base classes.

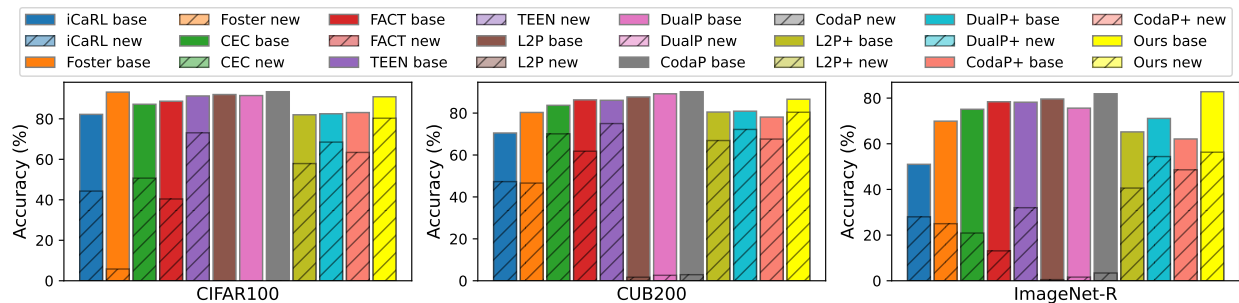


Figure 5: Comparison of baselines and ASP on detailed accuracy of base classes and new classes after the last task. ASP outperforms all baselines in terms of learning new classes using few-shot data while achieving competitive performance in maintaining performance on base classes.

6 Conclusion

It is important to leverage the recent large pre-trained models to perform few-shot class-incremental learning in real-world applications. In this work, we first point out the limitations of applying existing FSCIL methods and prompt-based CIL methods on FSCIL scenarios with large vision models. We further propose a new framework called ASP to learn generalized prompts to leverage the generalization of pre-trained ViT for incrementally learning new classes with limited data. Under the FSCIL setting, ASP outperforms baseline methods from classical CIL, FSCIL, and prompt-based CIL on three benchmark datasets.

Limitations: Possible limitations include the trade-off between learning new classes and maintaining performance in old ones. The ideal solution should improve both forward and backward transfer.

References

- [1] Gido M Van de Ven and Andreas S Tolias. Three scenarios for continual learning. *arXiv preprint arXiv:1904.07734*, 2019.
- [2] Yue Wu, Yinpeng Chen, Lijuan Wang, Yuancheng Ye, Zicheng Liu, Yandong Guo, and Yun Fu. Large scale incremental learning. In *Proceedings of the IEEE/CVF Conference on Computer Vision and Pattern Recognition (CVPR)*, June 2019.
- [3] Marc Masana, Xialei Liu, Bartłomiej Twardowski, Mikel Menta, Andrew D Bagdanov, and Joost Van De Weijer. Class-incremental learning: survey and performance evaluation on image classification. *IEEE Transactions on Pattern Analysis and Machine Intelligence*, 45(5):5513–5533, 2022.
- [4] Robert M French. Catastrophic forgetting in connectionist networks. *Trends in cognitive sciences*, 3(4):128–135, 1999.
- [5] Matthias De Lange, Rahaf Aljundi, Marc Masana, Sarah Parisot, Xu Jia, Aleš Leonardis, Gregory Slabaugh, and Tinne Tuytelaars. A continual learning survey: Defying forgetting in classification tasks. *IEEE transactions on pattern analysis and machine intelligence*, 44(7):3366–3385, 2021.
- [6] Zhizhong Li and Derek Hoiem. Learning without forgetting. *IEEE transactions on pattern analysis and machine intelligence*, 40(12):2935–2947, 2017.
- [7] Dipam Goswami, Yuyang Liu, Bartłomiej Twardowski, and Joost van de Weijer. Fecam: Exploiting the heterogeneity of class distributions in exemplar-free continual learning. *arXiv preprint arXiv:2309.14062*, 2023.
- [8] Le Sun, Mingyang Zhang, Benyou Wang, and Prayag Tiwari. Few-shot class-incremental learning for medical time series classification. *IEEE Journal of Biomedical and Health Informatics*, 2023.
- [9] Songsong Tian, Lusi Li, Weijun Li, Hang Ran, Xin Ning, and Prayag Tiwari. A survey on few-shot class-incremental learning. *Neural Networks*, 169:307–324, 2024.
- [10] Xiaoyu Tao, Xiaopeng Hong, Xinyuan Chang, Songlin Dong, Xing Wei, and Yihong Gong. Few-shot class-incremental learning. In *Proceedings of the IEEE/CVF Conference on Computer Vision and Pattern Recognition (CVPR)*, June 2020.
- [11] Guangyuan Shi, Jiabin Chen, Wenlong Zhang, Li-Ming Zhan, and Xiao-Ming Wu. Overcoming catastrophic forgetting in incremental few-shot learning by finding flat minima. *Advances in neural information processing systems*, 34:6747–6761, 2021.
- [12] Kai Zhu, Yang Cao, Wei Zhai, Jie Cheng, and Zheng-Jun Zha. Self-promoted prototype refinement for few-shot class-incremental learning. In *Proceedings of the IEEE/CVF Conference on Computer Vision and Pattern Recognition (CVPR)*, pages 6801–6810, June 2021.
- [13] Zhixiang Chi, Li Gu, Huan Liu, Yang Wang, Yuanhao Yu, and Jin Tang. Metafscil: A meta-learning approach for few-shot class incremental learning. In *Proceedings of the IEEE/CVF conference on computer vision and pattern recognition*, pages 14166–14175, 2022.
- [14] Anna Kukleva, Hilde Kuehne, and Bernt Schiele. Generalized and incremental few-shot learning by explicit learning and calibration without forgetting. In *Proceedings of the IEEE/CVF International Conference on Computer Vision (ICCV)*, pages 9020–9029, October 2021.
- [15] Ali Cheraghian, Shafin Rahman, Pengfei Fang, Soumava Kumar Roy, Lars Petersson, and Mehrtaash Harandi. Semantic-aware knowledge distillation for few-shot class-incremental learning. In *Proceedings of the IEEE/CVF conference on computer vision and pattern recognition*, pages 2534–2543, 2021.
- [16] Songlin Dong, Xiaopeng Hong, Xiaoyu Tao, Xinyuan Chang, Xing Wei, and Yihong Gong. Few-shot class-incremental learning via relation knowledge distillation. In *Proceedings of the AAAI Conference on Artificial Intelligence*, volume 35, pages 1255–1263, 2021.
- [17] Zhenyi Wang, Li Shen, Le Fang, Qiuling Suo, Donglin Zhan, Tiehang Duan, and Mingchen Gao. Meta-learning with less forgetting on large-scale non-stationary task distributions. In *European Conference on Computer Vision*, pages 221–238. Springer, 2022.
- [18] Zifeng Wang, Zizhao Zhang, Chen-Yu Lee, Han Zhang, Ruoxi Sun, Xiaoqi Ren, Guolong Su, Vincent Perot, Jennifer Dy, and Tomas Pfister. Learning to prompt for continual learning. In *Proceedings of the IEEE/CVF Conference on Computer Vision and Pattern Recognition*, pages 139–149, 2022.
- [19] Zifeng Wang, Zizhao Zhang, Sayna Ebrahimi, Ruoxi Sun, Han Zhang, Chen-Yu Lee, Xiaoqi Ren, Guolong Su, Vincent Perot, Jennifer Dy, et al. Dualprompt: Complementary prompting for rehearsal-free continual learning. In *European Conference on Computer Vision*, pages 631–648. Springer, 2022.

- [20] James Seale Smith, Leonid Karlinsky, Vyshnavi Gutta, Paola Cascante-Bonilla, Donghyun Kim, Assaf Arbelle, Rameswar Panda, Rogerio Feris, and Zsolt Kira. Coda-prompt: Continual decomposed attention-based prompting for rehearsal-free continual learning. In *Proceedings of the IEEE/CVF Conference on Computer Vision and Pattern Recognition*, pages 11909–11919, 2023.
- [21] Alexey Dosovitskiy, Lucas Beyer, Alexander Kolesnikov, Dirk Weissenborn, Xiaohua Zhai, Thomas Unterthiner, Mostafa Dehghani, Matthias Minderer, Georg Heigold, Sylvain Gelly, et al. An image is worth 16x16 words: Transformers for image recognition at scale. *arXiv preprint arXiv:2010.11929*, 2020.
- [22] Brian Lester, Rami Al-Rfou, and Noah Constant. The power of scale for parameter-efficient prompt tuning. In Marie-Francine Moens, Xuanjing Huang, Lucia Specia, and Scott Wen-tau Yih, editors, *Proceedings of the 2021 Conference on Empirical Methods in Natural Language Processing*, pages 3045–3059, Online and Punta Cana, Dominican Republic, November 2021. Association for Computational Linguistics.
- [23] Jason Wei, Xuezhi Wang, Dale Schuurmans, Maarten Bosma, Fei Xia, Ed Chi, Quoc V Le, Denny Zhou, et al. Chain-of-thought prompting elicits reasoning in large language models. *Advances in Neural Information Processing Systems*, 35:24824–24837, 2022.
- [24] Alexander A. Alemi, Ian Fischer, Joshua V. Dillon, and Kevin Murphy. Deep variational information bottleneck. In *International Conference on Learning Representations*, 2017.
- [25] Sylvestre-Alvise Rebuffi, Alexander Kolesnikov, Georg Sperl, and Christoph H Lampert. icarl: Incremental classifier and representation learning. In *Proceedings of the IEEE conference on Computer Vision and Pattern Recognition*, pages 2001–2010, 2017.
- [26] Rahaf Aljundi, Min Lin, Baptiste Goujaud, and Yoshua Bengio. Gradient based sample selection for online continual learning. *Advances in neural information processing systems*, 32, 2019.
- [27] David Rolnick, Arun Ahuja, Jonathan Schwarz, Timothy Lillicrap, and Gregory Wayne. Experience replay for continual learning. *Advances in Neural Information Processing Systems*, 32, 2019.
- [28] Zhenyi Wang, Li Shen, Tieshan Duan, Qiuling Suo, Le Fang, Wei Liu, and Mingchen Gao. Distributionally robust memory evolution with generalized divergence for continual learning. *IEEE Transactions on Pattern Analysis and Machine Intelligence*, 2023.
- [29] Zhenyi Wang, Yan Li, Li Shen, and Heng Huang. A unified and general framework for continual learning. In *The Twelfth International Conference on Learning Representations*, 2024.
- [30] Rahaf Aljundi, Francesca Babiloni, Mohamed Elhoseiny, Marcus Rohrbach, and Tinne Tuytelaars. Memory aware synapses: Learning what (not) to forget. In *Proceedings of the European conference on computer vision (ECCV)*, pages 139–154, 2018.
- [31] James Kirkpatrick, Razvan Pascanu, Neil Rabinowitz, Joel Veness, Guillaume Desjardins, Andrei A Rusu, Kieran Milan, John Quan, Tiago Ramalho, Agnieszka Grabska-Barwinska, et al. Overcoming catastrophic forgetting in neural networks. *Proceedings of the national academy of sciences*, 114(13):3521–3526, 2017.
- [32] Friedemann Zenke, Ben Poole, and Surya Ganguli. Continual learning through synaptic intelligence. In *International conference on machine learning*, pages 3987–3995. PMLR, 2017.
- [33] Geoffrey Hinton, Oriol Vinyals, and Jeff Dean. Distilling the knowledge in a neural network. *arXiv preprint arXiv:1503.02531*, 2015.
- [34] Vincenzo Lomonaco, Davide Maltoni, Lorenzo Pellegrini, et al. Rehearsal-free continual learning over small non-iid batches. In *CVPR Workshops*, volume 1, page 3, 2020.
- [35] Menglin Jia, Luming Tang, Bor-Chun Chen, Claire Cardie, Serge Belongie, Bharath Hariharan, and Ser-Nam Lim. Visual prompt tuning. In *European Conference on Computer Vision*, pages 709–727. Springer, 2022.
- [36] Liyuan Wang, Jingyi Xie, Xingxing Zhang, Mingyi Huang, Hang Su, and Jun Zhu. Hierarchical decomposition of prompt-based continual learning: Rethinking obscured sub-optimality. *arXiv preprint arXiv:2310.07234*, 2023.
- [37] Xiaoyu Tao, Xiaopeng Hong, Xinyuan Chang, Songlin Dong, Xing Wei, and Yihong Gong. Few-shot class-incremental learning. In *Proceedings of the IEEE/CVF Conference on Computer Vision and Pattern Recognition*, pages 12183–12192, 2020.
- [38] Zeyin Song, Yifan Zhao, Yujun Shi, Peixi Peng, Li Yuan, and Yonghong Tian. Learning with fantasy: Semantic-aware virtual contrastive constraint for few-shot class-incremental learning. In *Proceedings of the IEEE/CVF Conference on Computer Vision and Pattern Recognition*, pages 24183–24192, 2023.
- [39] Chi Zhang, Nan Song, Guosheng Lin, Yun Zheng, Pan Pan, and Yinghui Xu. Few-shot incremental learning with continually evolved classifiers. In *Proceedings of the IEEE/CVF Conference on Computer Vision and Pattern Recognition (CVPR)*, pages 12455–12464, June 2021.

- [40] Can Peng, Kun Zhao, Tianren Wang, Meng Li, and Brian C Lovell. Few-shot class-incremental learning from an open-set perspective. In *European Conference on Computer Vision*, pages 382–397. Springer, 2022.
- [41] Jake Snell, Kevin Swersky, and Richard Zemel. Prototypical networks for few-shot learning. *Advances in neural information processing systems*, 30, 2017.
- [42] Qi-Wei Wang, Da-Wei Zhou, Yi-Kai Zhang, De-Chuan Zhan, and Han-Jia Ye. Few-shot class-incremental learning via training-free prototype calibration. *arXiv preprint arXiv:2312.05229*, 2023.
- [43] Da-Wei Zhou, Fu-Yun Wang, Han-Jia Ye, Liang Ma, Shiliang Pu, and De-Chuan Zhan. Forward compatible few-shot class-incremental learning. In *Proceedings of the IEEE/CVF conference on computer vision and pattern recognition*, pages 9046–9056, 2022.
- [44] Yong Lin, Hanze Dong, Hao Wang, and Tong Zhang. Bayesian invariant risk minimization. In *Proceedings of the IEEE/CVF Conference on Computer Vision and Pattern Recognition*, pages 16021–16030, 2022.
- [45] Sebastian Ruder. An overview of gradient descent optimization algorithms. *arXiv preprint arXiv:1609.04747*, 2016.
- [46] Diederik P Kingma and Max Welling. Auto-encoding variational bayes. *arXiv preprint arXiv:1312.6114*, 2013.
- [47] Alexander A Alemi, Ian Fischer, Joshua V Dillon, and Kevin Murphy. Deep variational information bottleneck. *arXiv preprint arXiv:1612.00410*, 2016.
- [48] Xinwei Zhang, Jianwen Jiang, Yutong Feng, Zhi-Fan Wu, Xibin Zhao, Hai Wan, Mingqian Tang, Rong Jin, and Yue Gao. Grow and merge: A unified framework for continuous categories discovery. *Advances in Neural Information Processing Systems*, 35:27455–27468, 2022.
- [49] Chenxi Liu, Lixu Wang, Lingjuan Lyu, Chen Sun, Xiao Wang, and Qi Zhu. Deja vu: Continual model generalization for unseen domains, 2023.
- [50] Da-Wei Zhou, Han-Jia Ye, De-Chuan Zhan, and Ziwei Liu. Revisiting class-incremental learning with pre-trained models: Generalizability and adaptivity are all you need, 2023.
- [51] Alex Krizhevsky, Geoffrey Hinton, et al. Learning multiple layers of features from tiny images. 2009.
- [52] Catherine Wah, Steve Branson, Peter Welinder, Pietro Perona, and Serge Belongie. The caltech-ucsd birds-200-2011 dataset. 2011.
- [53] Dan Hendrycks, Steven Basart, Norman Mu, Saurav Kadavath, Frank Wang, Evan Dorundo, Rahul Desai, Tyler Zhu, Samyak Parajuli, Mike Guo, et al. The many faces of robustness: A critical analysis of out-of-distribution generalization. In *Proceedings of the IEEE/CVF International Conference on Computer Vision*, pages 8340–8349, 2021.
- [54] Adam Paszke, Sam Gross, Francisco Massa, Adam Lerer, James Bradbury, Gregory Chanan, Trevor Killeen, Zeming Lin, Natalia Gimelshein, Luca Antiga, et al. Pytorch: An imperative style, high-performance deep learning library. *Advances in neural information processing systems*, 32, 2019.
- [55] Fu-Yun Wang, Da-Wei Zhou, Han-Jia Ye, and De-Chuan Zhan. Foster: Feature boosting and compression for class-incremental learning. In *European conference on computer vision*, pages 398–414. Springer, 2022.
- [56] Kaiming He, Xiangyu Zhang, Shaoqing Ren, and Jian Sun. Deep residual learning for image recognition. In *Proceedings of the IEEE conference on computer vision and pattern recognition*, pages 770–778, 2016.
- [57] Marco D’Alessandro, Alberto Alonso, Enrique Calabrés, and Mikel Galar. Multimodal parameter-efficient few-shot class incremental learning. In *Proceedings of the IEEE/CVF International Conference on Computer Vision (ICCV) Workshops*, pages 3393–3403, October 2023.
- [58] In-Ug Yoon, Tae-Min Choi, Sun-Kyung Lee, Young-Min Kim, and Jong-Hwan Kim. Image-object-specific prompt learning for few-shot class-incremental learning. *arXiv preprint arXiv:2309.02833*, 2023.
- [59] Alec Radford, Jong Wook Kim, Chris Hallacy, Aditya Ramesh, Gabriel Goh, Sandhini Agarwal, Girish Sastry, Amanda Askell, Pamela Mishkin, Jack Clark, et al. Learning transferable visual models from natural language supervision. In *International conference on machine learning*, pages 8748–8763. PMLR, 2021.
- [60] Naftali Tishby, Fernando C Pereira, and William Bialek. The information bottleneck method. *arXiv preprint physics/0004057*, 2000.

Appendix

A Experimental Details

In this section, we illustrate the details of datasets and implementation of baselines. Furthermore, the detailed experimental results on CUB200 are provided.

A.1 Dataset Details

We follow previous FSCIL works [43, 42] to use CIFAR100 [51] and CUB200-2011 [52] datasets. As the ViT backbone is pre-trained on ImageNet, we follow previous prompt-based CIL works [18, 19] to use ImageNet-R [53] as another benchmark dataset. CIFAR100 contains 100 classes with 500 training images and 100 testing images per class. The CUB200-2011 is a fine-grained dataset with 200 classes of different birds. It contains 5,994 samples for training and 5,794 samples for testing. The ImageNet-R contains 16 different renditions of 200 ImageNet classes and the total number of images is 30,000. We follow previous works [43, 42] to split the classes as base and new classes. For the new classes under the k -shot setting, k images are randomly chosen from each class for training.

A.2 Baseline Details

For the classical CIL methods iCaRL [25] and Foster [55], we follow the original implementation and equip iCaRL with a rehearsal buffer of size 200. For FSCIL baselines CEC, FACT and TEEN, we replace the original ResNet backbone with the same ViT-B/16-1K [21] we used for ASP. The other operations are kept the same as the original implementations. As we find that the original implementation of prompt-based approaches performs badly under the FSCIL setting, we replace the original classifier head with the class mean to construct the Prototypical Network, and denote them as L2P+, DualP+ and CodaP+. For a fair comparison, all methods are tuned 20 epochs on base classes.

A.3 Detail Results for Main Paper

In the main paper, we only provide the Top-1 accuracy of CUB200 in Figure 1, here we provide the detailed comparison between baselines and ASP on CUB200, which is shown in Table 5. Like CIFAR100 and ImageNet-R, ASP achieves the best on A_{avg} , PD and HAcc, surpassing the second best by 0.7%, 3.2% and 3.2% respectively. In addition, ASP also achieves the best A_{10} of 83.5% after the last task, outperforms the second best by 2.9%.

Table 5: Detailed Top-1 accuracy A_t in each incremental task, average accuracy A_{avg} , performance dropping rate (PD) and Harmonic Accuracy (HAcc) on CUB200 dataset. \uparrow means higher is better, and \downarrow means lower is better.

Method	Accuracy A_t in each task (%) \uparrow											A_{avg} \uparrow	PD \downarrow	HAcc \uparrow
	0	1	2	3	4	5	6	7	8	9	10			
iCaRL	92.4	82.3	71.7	62.9	64.6	62.9	60.8	60.3	58.4	55.7	58.9	66.4	33.5	56.4
Foster	93.0	86.4	80.4	74.5	72.9	69.3	68.5	66.0	65.9	65.0	63.4	73.2	29.6	58.8
CEC	84.8	82.5	81.4	78.5	79.3	77.8	77.4	77.6	77.2	76.9	76.8	79.1	7.9	76.2
FACT	87.3	84.2	82.1	78.1	78.4	76.3	75.4	75.5	74.4	74.1	73.9	78.2	13.4	72.0
TEEN	89.0	86.5	85.9	83.3	83.3	82.2	82.1	80.4	80.5	80.1	80.6	83.1	9.4	80.2
L2P	87.8	81.3	74.2	68.9	63.4	59.2	55.8	51.9	49.0	46.3	44.3	62.0	43.5	3.3
DualP	88.9	82.6	75.3	69.6	64.5	60.4	56.8	53.0	50.0	47.5	45.5	63.1	43.4	5.0
CodaP	89.9	83.1	75.8	70.2	65.1	61.0	57.5	53.7	50.7	48.3	46.2	63.8	43.7	5.7
L2P+	82.4	81.2	79.0	76.8	76.2	74.7	74.1	74.1	72.7	73.0	73.6	76.2	8.7	73.0
DualP+	83.5	82.2	80.9	79.5	78.6	77.0	76.3	77.0	75.7	76.1	76.5	78.5	7.1	76.3
CodaP+	79.6	78.1	76.4	75.6	75.0	73.1	72.5	72.8	72.0	72.4	72.9	74.6	6.8	72.5
ours	87.1	86.0	84.9	83.4	83.6	82.4	82.6	83.0	82.6	83.0	83.5	83.8	3.6	83.4

A.4 Comparison with Multi-modality Backbone

Instead of using ResNet [56] as the backbone in classical FSCIL methods or using ViT [21] as the backbone in prompt-based CIL methods and ASP, some recent works utilize large multi-modality models to address the FSCIL scenario. CPE-CLIP [57] and IOS [58] use OpenAI CLIP [59] as the backbone. Their CLIP backbone uses the ViT-Base

Table 6: Detailed Top-1 accuracy A_t in each incremental task, average accuracy A_{avg} and performance dropping rate (PD) on CIFAR100 dataset. \uparrow means higher is better, and \downarrow means lower is better.

Method	Accuracy A_t in each task (%) \uparrow									A_{avg} \uparrow	PD \downarrow
	0	1	2	3	4	5	6	7	8		
CPE-CLIP	87.8	85.9	84.9	82.9	82.6	82.4	82.3	81.4	80.5	83.4	7.3
Ours	92.2	90.7	90.0	88.7	88.7	88.2	88.2	87.8	86.7	89.0	5.5

Table 7: Detailed Top-1 accuracy A_t in each incremental task, average accuracy A_{avg} and performance dropping rate (PD) on CUB200 dataset. \uparrow means higher is better, and \downarrow means lower is better.

Method	Accuracy A_t in each task (%) \uparrow										A_{avg} \uparrow	PD \downarrow	
	0	1	2	3	4	5	6	7	8	9			10
CPE-CLIP	81.6	78.5	76.7	71.9	71.5	70.2	67.7	66.5	65.1	64.5	64.6	70.8	17.0
ours	87.1	86.0	84.9	83.4	83.6	82.4	82.6	83.0	82.6	83.0	83.5	83.8	3.6

model as the image encoder, which is the same size as our experimental setting. Thus, the model backbones have comparable capability, and we compare their performance with ASP under the same FSCIL setting. As for now, we only have the detailed results reported by the original paper of CPE-CLIP, we compare it with ASP on the CIFAR100 and CUB200 datasets and show the result in Table 6 and Table 7. ASP significantly outperforms CPE-CLIP on all metrics.

B Detailed Derivation of IB Loss

The approach of *Information Bottleneck* was first proposed by work [60], where the goal is to learn an encoding feature P that is maximally expressive about the label Y while being maximally compressive about the input X :

$$\mathcal{L}_{IB} = I(\mathcal{P}; \mathcal{X}) - \gamma I(\mathcal{P}; \mathcal{Y}) \quad (20)$$

In general, it is computationally challenging to calculate the mutual information $I(\cdot)$. We follow the Variational Information Bottleneck method [47] to construct a lower bound on the IB objective in Equation 20.

Following standard practice in the IB literature, we assume that the joint distribution $P(\mathcal{X}, \mathcal{Y}, \mathcal{P})$ factors as follows:

$$P(\mathcal{X}, \mathcal{Y}, \mathcal{P}) = P(\mathcal{P}|\mathcal{X}, \mathcal{Y})P(\mathcal{Y}|\mathcal{X})P(\mathcal{X}) = P(\mathcal{P}|\mathcal{X})P(\mathcal{Y}|\mathcal{X})P(\mathcal{X}) \quad (21)$$

where we assume $P(\mathcal{P}|\mathcal{X}, \mathcal{Y}) = P(\mathcal{P}|\mathcal{X})$ based on the Markov chain. We then write $I(\mathcal{P}; \mathcal{Y})$ out in full:

$$I(\mathcal{P}, \mathcal{Y}) = \int d\mathbf{y} d\mathbf{p} P(\mathbf{y}, \mathbf{p}) \log \frac{P(\mathbf{y}, \mathbf{p})}{P(\mathbf{y})P(\mathbf{p})} = \int d\mathbf{y} d\mathbf{z} P(\mathbf{y}, \mathbf{p}) \log \frac{P(\mathbf{y}|\mathbf{p})}{P(\mathbf{y})} \quad (22)$$

where $P(\mathbf{y}|\mathbf{p})$ is defined as follows:

$$P(\mathbf{y}|\mathbf{p}) = \int d\mathbf{x} P(\mathbf{x}, \mathbf{y}|\mathbf{p}) = \int d\mathbf{x} P(\mathbf{y}|\mathbf{x})P(\mathbf{x}|\mathbf{p}) = \int d\mathbf{x} \frac{P(\mathbf{y}|\mathbf{x})P(\mathbf{p}|\mathbf{x})P(\mathbf{x})}{P(\mathbf{p})} \quad (23)$$

Let $q(\mathbf{y}|\mathbf{p})$ be a variational approximation to $P(\mathbf{y}|\mathbf{p})$. As the Kullback Leibler divergence is always positive, we have

$$\mathbb{KL}[P(\mathcal{Y}|\mathcal{P}), q(\mathcal{Y}|\mathcal{P})] \geq 0 \implies \int d\mathbf{y} P(\mathbf{y}|\mathbf{p}) \log P(\mathbf{y}|\mathbf{p}) \geq \int d\mathbf{y} P(\mathbf{y}|\mathbf{p}) \log q(\mathbf{y}|\mathbf{p}) \quad (24)$$

and hence

$$I(\mathcal{P}, \mathcal{Y}) \geq \int d\mathbf{y} d\mathbf{z} P(\mathbf{y}, \mathbf{p}) \log \frac{q(\mathbf{y}|\mathbf{p})}{P(\mathbf{y})} \quad (25)$$

$$= \int d\mathbf{y} d\mathbf{p} P(\mathbf{y}, \mathbf{p}) \log q(\mathbf{y}|\mathbf{p}) - \int d\mathbf{y} P(\mathbf{y}) \log P(\mathbf{y}) \quad (26)$$

$$= \int d\mathbf{y} d\mathbf{p} P(\mathbf{y}, \mathbf{p}) \log q(\mathbf{y}|\mathbf{p}) + H(\mathcal{Y}) \quad (27)$$

The entropy of labels $H(\mathcal{Y})$ is independent of our optimization procedure, and thus can be ignored.

Leveraging our Markov assumption, we can rewrite $P(\mathbf{y}, \mathbf{p}) = \int d\mathbf{x} P(\mathbf{x}, \mathbf{y}, \mathbf{p}) = \int d\mathbf{x} P(\mathbf{x})P(\mathbf{y}|\mathbf{x})P(\mathbf{p}|\mathbf{x})$ in Equation 27, which gives us a new lower bound on the first term of our objective:

$$I(Z, Y) \geq \int d\mathbf{x} d\mathbf{y} dz P(\mathbf{x})P(\mathbf{y}|\mathbf{x})P(\mathbf{p}|\mathbf{x}) \log q(\mathbf{y}|\mathbf{p}). \quad (28)$$

We now consider the term $\gamma I(\mathcal{P}, \mathcal{X})$:

$$I(\mathcal{P}, \mathcal{X}) = \int d\mathbf{p} d\mathbf{x} P(\mathbf{x}, \mathbf{p}) \log \frac{P(\mathbf{p}|\mathbf{x})}{P(\mathbf{p})} \quad (29)$$

$$= \int d\mathbf{p} d\mathbf{x} P(\mathbf{x}, \mathbf{p}) \log P(\mathbf{p}|\mathbf{x}) - \int d\mathbf{p} P(\mathbf{p}) \log P(\mathbf{p}). \quad (30)$$

In general, computing the marginal distribution of \mathcal{P} , $P(\mathbf{p}) = \int d\mathbf{x} P(\mathbf{p}|\mathbf{x})P(\mathbf{x})$, might be difficult. We let $r(\mathbf{p})$ be a variational approximation to this marginal. Since $\mathbb{KL}[P(\mathcal{P}), r(\mathcal{P})] \geq 0 \implies \int d\mathbf{p} P(\mathbf{p}) \log P(\mathbf{p}) \geq \int d\mathbf{p} P(\mathbf{p}) \log r(\mathbf{p})$, we have the following upper bound:

$$I(\mathcal{P}, \mathcal{X}) \leq \int d\mathbf{x} d\mathbf{p} P(\mathbf{x})P(\mathbf{p}|\mathbf{x}) \log \frac{P(\mathbf{p}|\mathbf{x})}{r(\mathbf{p})} \quad (31)$$

Combining both of these bounds we have that

$$\begin{aligned} I(\mathcal{P}, \mathcal{Y}) - \gamma I(\mathcal{P}, \mathcal{X}) &\geq \int d\mathbf{x} d\mathbf{y} d\mathbf{p} P(\mathbf{x})P(\mathbf{y}|\mathbf{x})P(\mathbf{p}|\mathbf{x}) \log q(\mathbf{y}|\mathbf{p}) \\ &\quad - \gamma \int d\mathbf{x} d\mathbf{p} P(\mathbf{x})P(\mathbf{p}|\mathbf{x}) \log \frac{P(\mathbf{p}|\mathbf{x})}{r(\mathbf{p})} \end{aligned} \quad (32)$$